Eur. Phys. J. D (2021)75:140
https://doi.org/10.1140/epjd/s10053-021-00145-0

THE EUROPEAN PHYSICAL JOURNAL D

Regular Article – Atomic Physics

Electron capture nuclear decay rate under compression in a confined environment

A. Ray[1,a], P. Das[1,2], A. K. Sikdar[1], S. Pathak[1,2], N. Aquino[3], Mayra Lozano-Espinosa[4], and A. N. Artemyev[5]

[1] Variable Energy Cyclotron Center, 1/AF, Bidhannagar, Kolkata 700064, India
[2] Homi Bhabha National Institute Training School Hostel, Anushaktinagar, Mumbai 400094, India
[3] Departmento de Física, Universidad Autónoma Metropolitana-Iztapalapa, Av. San Rafael Atlixco186, C.P. 09340 Mexico, DF, Mexico
[4] CONACYT - Universidad Autónoma Metropolitana-Cuajimalpa, Av. Vasco de Quiroga 4871, Santa Fe Cuajimalpa, C.P. 05300 Mexico, DF, Mexico
[5] Institute of Physics and CINSaT, University of Kassel, Heinrich-Plett-St. 40, 34132 Kassel, Germany

Received 21 December 2020 / Accepted 2 April 2021

Abstract. We have calculated the effect of compressing the radioactive atoms in the crystal lattice environments on their electron capture nuclear decay rates. The electronic structure calculations of solids using the density functional techniques have been used to calculate the change of electron density at the nuclei and the corresponding change of electron capture nuclear decay rate of the radioactive atoms confined to the interstitial spaces of different crystal lattices. The effects of finite nuclear size and vacuum polarization were considered in the calculations. It has been found that the calculations significantly underpredict the experimentally measured increase of electron capture nuclear decay rate under compression. The increase of decay rate due to compression-induced quantum anti-Zeno effect is generally believed to be very small because of very short duration of initial nonexponential decay time for the nuclear decays. However, this effect could be observable for the electron capture nuclear decay of ^{163}Ho, because of its very low decay energy. Moreover, certain models of quantum measurement indicate much longer initial nonexponential decay time and the corresponding implication on the increase of decay rate under compression is still not known. It is important to understand the large discrepancy between the measured and calculated increase of electron capture nuclear decay rate under compression and the associated role of quantum anti-Zeno effect because of their possible implications in various astrophysical and geophysical calculations.

1 Introduction

The study of atoms in a confined environment is of general interest and has wide-spread applications in many areas [1]. One might simulate the effect of pressure on an atom by putting it in a confined environment and as a result the electron density at the atomic nucleus is expected to increase. A type of radioactive decay known as the electron capture nuclear decay takes place when the atomic nucleus captures an electron and is converted to a nucleus of lower atomic number along with the emission of a neutrino. Although the radioactive decay is generally known to be independent of the external environment, the electron capture nuclear decay rate (λ_{EC}) is susceptible to the external environment because it is proportional to the electron density at the nucleus [2]. The electron-capture nuclear decay rate (λ_{EC}) is given by [2] the formula

$\lambda_{EC} = \frac{(E_\nu)^2}{\pi c^3 \hbar^4} g^2 |H_{fi}|^2 |\psi_e(0)|^2$, where $\psi_e(0)$ is the electronic wave function at the nucleus and hence $\rho(0) = |\psi_e(0)|^2$ is the electron density at the nucleus. H_{fi} is the nuclear matrix element, g is the weak interaction coupling constant, E_ν is the kinetic energy of the emitted neutrino, c is the speed of light in vacuum and $\hbar = \frac{h}{2\pi}$, where h is the Planck's constant. Since H_{fi}, g and E_ν are independent of the external environment, we obtain

$$\lambda_{EC} \propto |\psi_e(0)|^2 \text{ or } \lambda_{EC} \propto \rho(0) \tag{1}$$

We may write

$|\psi_e(0)|^2 = |\psi_{1s}(0)|^2 + |\psi_{2s}(0)|^2 + \cdots + |\psi_V(0)|^2$, where $|\psi_{1s}(0)|^2$, $|\psi_{2s}(0)|^2$ and $|\psi_V(0)|^2$ are 1s, 2s and valence (s-orbital) electron densities at the nucleus respectively. The external environment could affect the valence electronic orbitals, thus changing $|\psi_e(0)|^2$ and

Contribution to the Topical Issue "Atoms and Molecules in a Confined Environment" edited by C. N. Ramachandran, Vincenzo Aquilanti, Henry Ed Montgomery, Narayanasami Sathyamurthy.

[a] e-mail: amlanray2016@gmail.com (corresponding author)

Published online: 27 April 2021

λ_{EC}. Hence, the small changes of the electron capture nuclear β-decay rate in different chemical environments are expected, because the valence electrons of the radioactive atom are affected by the chemical environments. The electron capture nuclear decay rate of ^{7}Be is most susceptible to such changes [3] as the 2s valence orbital electrons of ^{7}Be contribute about 3.3% of the total electron density at the nucleus. In the case of higher Z elements, such an effect is expected to be negligible because of the negligible overlap of the valence electrons at the nucleus. The change of electron capture nuclear decay rate of ^{7}Be in different chemical environments has been observed experimentally [3–8] and the electron affinity of the surrounding medium plays an important role in affecting these changes. For example, ^{7}Be implanted in a medium of high electron affinity such as gold (Au) loses more 2s electrons compared to the ^{7}Be implanted in a medium of low electron affinity such as aluminum (Al). As a result, the decay rate of ^{7}Be in Au becomes slower compared to that of ^{7}Be implanted in Al. Quantitative calculations [7,9,10] using density functional techniques provide a reasonable explanation of the observed changes of the decay rate of ^{7}Be implanted in the media of different electron affinities.

The effect of compression in a crystal lattice environment could also change the electron capture nuclear decay rate by affecting the orbital electronic configuration of the radioactive atoms and in this paper, we focus on this aspect. In order to study the effect of compression on the decay rate of ^{7}Be, external pressure could be applied to a ^{7}Be compound by a diamond anvil cell or ^{7}Be could be implanted in the interstitial space of a small crystal lattice. In these cases, 2s valence electrons of ^{7}Be atom would be pushed inward towards the nucleus, increasing the 2s electron density at the nucleus and the decay rate of ^{7}Be. The 2s electrons that are pushed inward screen the nuclear charge as seen by 1s orbital electrons to some extent, resulting in a small decrease of 1s electron density at the nucleus. It turns out that the net effect is a small increase of the total electron density at the nucleus, resulting in a slight increase of the decay rate of ^{7}Be under compression. The electron-capture nuclear decay rate of heavier atoms (such as ^{109}In and ^{110}Sn) containing many electronic orbitals should also increase under compression for similar reasons, but the percentage increase is expected to be much smaller compared to that of ^{7}Be under similar compression.

However, the available measurements of the electron capture nuclear decay rate of radioactive atoms (such as ^{7}Be,^{109}In and ^{110}Sn) under compression shows a significantly higher percentage increase of the decay rate compared to the results of the electronic structure calculations of solids, performed by using density functional and Hartree-Fock techniques. In this paper, we have performed calculations including all known standard effects such as the finite nuclear size, possibility of any pressure-induced phase transition and quantum electrodynamics (QED). However, significant discrepancies between the calculations and observations persist. We discuss about the possible increase of decay rate due to quantum anti-Zeno effect and the importance of understanding the origin of the large discrepancies because of its implications in astrophysical and geophysical calculations.

2 Available measurements

2.1 ^{7}BeO under compression

The change of electron capture nuclear decay rate of ^{7}Be under compression could be studied experimentally either by directly applying external pressure on a ^{7}Be compound or implanting ^{7}Be in the interstitial space of a small crystal lattice. Hensley et al. [11] measured the fractional change of decay rate of ^{7}Be by directly applying external pressure up to 27 GPa on ^{7}BeO crystal and obtained the relationship:
$\frac{\Delta\lambda}{\lambda} = (2.2 \pm 0.1) \times 10^{-4}P$ for $P \leq 27$ GPa, where$\Delta\lambda/\lambda$ is the fractional change of decay rate and P is the external pressure in the Gigapascal (GPa) unit. Lin-gun and Chih-An Huh [12] compressed $^{7}Be(OH)_2$ gel under high pressure up to 44.2 GPa and found that that the increase of decay rate of ^{7}Be with the applied pressure (P) followed the quadratic equation:
$\frac{\Delta\lambda}{\lambda} = 4.87 \times 10^{-4}P - (5.9 \times 10^{-7}P^2)$ for $P \leq 44.2$ GPa, where the external pressure P is in the GPa unit. The experimental result of Hensley et al. [11] and that of Lin-gun and Chih-An Huh [12] are in qualitative agreement with each other, even though one work was done using ^{7}BeO lattice [11] and the other one using amorphous $^{7}Be(OH)_2$ gel [12].

2.2 ^{7}Be implantation in the small and large lattices.

Another way to study the effect of compression on the electron capture nuclear decay rate is by implanting the electron capturing radioactive atoms in the interstitial spaces of a small and large crystal lattice. The outer electronic orbitals of the implanted electron capturing radioactive atoms confined to the interstitial spaces of the smaller lattice would experience higher compression, thus increasing the electron density at the nucleus and hence, the electron-capture nuclear decay rate. However, the electron affinity of the surrounding host medium would also affect the valence electronic orbital of the implanted atoms, thus affecting the decay rate of the implanted electron-capturing nuclei. Hence, the extraction of the effect of lattice compression on the electron capture nuclear decay rate becomes difficult. Cheng-Bo *et al.* [13] implanted ^{7}Be in the interstitial spaces of the small palladium (Pd) lattices (lattice constant = 3.89Å; electron affinity = 0.56 eV) and larger gold (Au) lattices (lattice constant = 4.08Å; electron affinity = 2.3 eV) [14] and found that the decay rate of ^{7}Be was faster in Pd compared to that in Au by $\frac{\Delta\lambda}{\lambda} = (0.8 \pm 0.2)\%$. They also implanted ^{7}Be in the interstitial spaces of the small platinum (Pt) lattices

(lattice constant = 3.92 Å; electron affinity = 2.1 eV) and larger aluminum (Al)lattices (lattice constant = 4.05 Å; electron affinity = 0.4 eV) [14] and found that the decay rate of ^{7}Be in Pt was faster than that in Al by $\frac{\Delta\lambda}{\lambda} = (0.17 \pm 0.13)\,\%$. Although ^{7}Be is expected to experience higher compression in Pd and Pt compared to that in Au and Al respectively, it is difficult to disentangle the effect of lattice compression because of the vastly different electron affinities of Au and Pt compared to those of Pd and Al respectively.

So, Ray et al. [15] implanted ^{7}Be in Pd and Pb [face-centered cubic lattice: lattice constant = 4.95Å; electron affinity = 0.37 eV] [14] and found that the decay rate of ^{7}Be is faster in the smaller Pd lattice compared that in the larger Pb lattice by $(0.82 \pm 0.16)\%$. Since the electron affinities of both Pd and Pb are very small and similar, the observed increase of decay rate in the smaller Pd lattice could be attributed to the effect of compression on ^{7}Be atom in the smaller confinement.

2.3 Implantation of high Z elements in the small and large lattices

In the case of high Z elements, ^{109}In and ^{110}Sn were implanted [16] in the interstitial spaces of the small Au lattices and larger Pb lattice. The ground states of both the ^{109}In and ^{110}Sn nuclei decay predominantly by orbital electron capture. It was found that the decay rate of ^{109}In implanted in Au lattice was $(1.00 \pm 0.17)\%$ faster compared to when ^{109}In had been implanted in Pb. The measurements on ^{110}Sn showed that its decay rate was faster in Au by $(0.48 \pm 0.25)\%$ compared to that in Pb. The valence electronic configuration of In and Sn are $5s^2 5p^1$ and $5s^2 5p^2$ respectively and their overlap at the nucleus is extremely small ($\approx 10^{-4}\%$) compared to that of the inner electronic orbitals. Since the electron affinity of the surrounding medium primarily affects the valence orbitals of the implanted ion, the effect of higher electron affinity of Au (electron affinity = 2.31 eV [14]) compared to that of Pb (electron affinity = 0.35 eV [14]) would have negligible effect on the decay rate of the implanted ^{109}In and ^{110}Sn ions. So, the observed increase of decay rate of ^{109}In and ^{110}Sn in the smaller Au lattice compared to that of in Pb could be attributed to the effect of lattice compression.

3 Calculations

3.1 ^{7}BeO under compression

We have calculated electron density at the nucleus as a function of the lattice parameters of beryllium oxide lattice using WIEN2k density functional code [17,18]. This code performs electronic structure calculations of solids. Point nuclei and relativistic Dirac wave functions for the electrons were used for all these calculations. The experimentally obtained wurzite lattice structure and the corresponding lattice parameters [19] of beryllium oxide (BeO) were taken as the initial lattice parameters before the application of any external pressure. These lattice parameters [19] give the initial lattice volume as V = 25.17(Å)^3. In the calculations, the effect of compression was studied by proportionately reducing the lattice parameters of BeO lattice without distorting the lattice structure and the change of electron density at ^{7}Be nucleus was calculated using the density functional code WIEN2k [17,18]. The calculations are based on the full-potential (linearized) augmented plane-wave and local orbitals method. The exchange-correlation energy has been included in the calculations and it is a functional of the local electron density. The generalized gradient approximation with the parametrization of Perdew, Burke and Ernzerhof (PBE) [20,21] was used for the exchange-correlation functional. The code calculated electron density at different radial distances from the nucleus. The electron density theoretically becomes infinity exactly at the point nucleus ($r = 0$) for the relativistic Dirac wave function and it decreases rapidly at the points away from the atomic nucleus. However, the fractional increase of the electron density $[\Delta\rho(0)/\rho(0)]$ due to the proportionate reduction of the lattice parameters of ^{7}BeO lattice (compressional effect) remains about the same (within 0.01%) at the points 2 to 50 fm away from the atomic nucleus. All the calculations have been done by taking the electron density at a point 2.6 fm away from the point atomic nucleus and it has been denoted by $\rho(0)$. The total energy convergence was better than 1 meV/atom and the charge convergence in the muffin-tin sphere was on the order of 10^{-3}e/(Bohr unit)^3. In the case of application of external pressure, the lattice was relaxed so that the forces on the atoms were about 1mRy/Bohr Unit. We find that for the ^{7}BeO lattice, the fractional increase of the electron density at beryllium nucleus $[\Delta\rho(0)/\rho(0)]$ depends on the fractional change of the volume of ^{7}BeO lattice (Δ V/V). The relationship between the applied external pressure (P) and fractional change of lattice volume (Δ V/V) has been taken from the calculated isotherm at 25° C [22] and the values of $[\Delta\rho(0)/\rho(0)]$ for different values of P were determined. Hence using Eq. (1), we obtain the percentage increase of electron capture nuclear decay rate $\left[\frac{\Delta\lambda_{EC}}{\lambda_{EC}} \times 100\%\right]$ with the external pressure (P). In Fig. 1, we show the results of our calculations along with the earlier calculations by Lee and Steinle-Neumann [10] and the corresponding data points for the ^{7}BeO crystal. There is a good agreement between our calculations and the previous calculation [10]. The small difference between the two calculations is probably because we have used smaller wurzite lattice parameters, as obtained experimentally [19], whereas the earlier calculations [10] used larger hexagonal close pack structure. Our calculated results could be approximated by the linear relationship

$$\frac{\Delta\lambda}{\lambda} \approx 0.6 \times 10^{-4} P \text{ for } P \leq 27\,\text{GPa}.$$

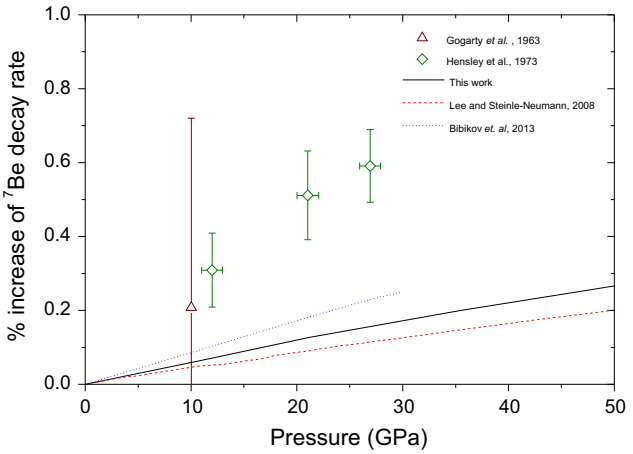

Fig. 1 Experimental data points for the applied external pressure (P in GPa unit) on ^{7}BeO crystal versus the percentage increase of λ_{EC} for ^{7}Be along with the results of the WIEN2k density functional calculations from this work and Ref. [10] as well as the results from the Hartree-Fock calculations from Ref. [23]

Bibikov et al. [23] performed Hartree-Fock calculations using wurzite lattice structure of BeO and included the effect of electron correlations by including the second-order Møller-Plesset perturbation contribution [24] to the ground state energy. They employed the resolution of identity scheme (RI) for computing two electron matrix elements of Coulomb repulsion, thus effectively including explicitly correlated R12/F12 scheme for electronic structure [24,25]. In Fig. 1, the results of Bibikov et al.'s calculations have been overlayed to compare with the density functional calculations. We find that all the calculations are reasonably close to one another and they underpredict the experimental results by large factors.

Bibikov et al. [23] attempted to explain the discrepancy by a phase transition of BeO lattice at 27 GPa pressure from the wurzite to rock-salt structure. However, Mori et al. [26] performed a high-pressure x-ray structural study of BeO crystal and observed phase transformation from the wurtzite to the rock-salt structure at an externally applied pressure of (137 ± 5) GPa, in good agreement with the theoretical value of 139 GPa. Earlier work by Jephcoat et al. [27] also supported the conclusion that the phase transformation of BeO crystal from the wurtzite to the rock-salt structure took place at an external pressure >100 GPa. So, there would be no pressure-induced phase transformation of BeO lattice structure at the maximum applied pressure of 27 GPa, where the decay rate change was measured by Hensley et al. [11]. Moreover, as shown earlier [28], a pressure induced phase transformation of BeO lattice from wurtzite to rock-salt structure would reduce the rate of increase of electron capture decay rate with pressure, contrary to the experimental results. So, both the density functional and Hartree-Fock calculations underpredict by a large factor the observed increase of electron-capture nuclear decay rate of ^{7}Be under compression.

3.2 ^{7}Be implantation in the small and large lattices.

In order to see the effect of lattice compression from Cheng-Bo et al.'s [13] experiment, we have to first determine the loss of 2s valence electrons of ^{7}Be atoms implanted in Au versus Pd lattice and Pt versus Al. Both Au and Pd lattices are face-centered cubic (FCC) with the lattice constants = 4.08Å and 3.89Å respectively. The electron affinities of Au and Pd are 2.31 eV and 0.56 eV respectively. Similarly, both Pt and Al lattices are FCC lattices with the lattice constant = 3.92Å and 4.05Å respectively. The electron affinities of Pt and Al are 2.12 eV and 0.43 eV respectively [14]. We used the density functional code TB-LMTO [29,30] to calculate the average number of 2s valence electrons of ^{7}Be implanted in a crystal lattice. Relativistic Dirac wave functions were used for the orbital electrons and ^{7}Be atoms were placed in either the octahedral or tetrahedral interstitial spaces of the lattice maintaining the periodicity of the lattice structure. Considering that the number of tetrahedral positions is twice that of octahedral positions, we calculate the weighted average of the total number of 2s electrons of ^{7}Be implanted in Pd and Au as well as in Pt and Al. The number of 2s electrons of ^{7}Be implanted in these media differs primarily because of the different electron affinities of these media. From the calculated differences of the average number of 2s orbital electrons of implanted ^{7}Be atom in different media, we obtain that the decay rate of ^{7}Be in Pd would be faster by about 0.3% compared to that in Au and the decay rate of ^{7}Be in Al would be faster than that in Pt by about 0.4%. These results reflect the effect of higher electron affinities of Au and Pt compared to those of Pd and Al. However, Cheng-Bo et al. [13] measured significantly larger increase of decay rate (0.8 ± 02)% of ^{7}Be in Pd compared to that in Au, thus indicating that the effect of lattice compression in the smaller Pd lattice compared to that in Au might increase ^{7}Be decay rate by ~ 0.5%. Similarly, the decay rate of ^{7}Be in Al should have been faster by about 0.4% compared to that in Pt due to the effect of the electron affinity. The observed slight decrease (-0.17 ± 0.13)% [13] of decay rate of ^{7}Be in Al compared to that in Pt indicates that the effect of lattice compression in the smaller Pt lattice compared to that in Al might increase ^{7}Be decay rate by ~ 0.5%. Considering the experimental uncertainties and the uncertainties of TB-LMTO density functional calculations, it is not possible to extract quantitatively the effect of lattice compression from such measurements with a reasonable confidence. However, we get a qualitative evidence for the increase of ^{7}Be decay rate under compression. We have summarized our results in Table -1, showing the combined effect of the electron affinity and lattice compression on the change of the decay rate of ^{7}Be.

Table 1 Combined effect of electron affinity and lattice compression on the change of ^{7}Be decay rate

Increase of ^{7}Be decay rate in	Increase of ^{7}Be decay rate due to electron affinity [TB-LMTO calculations]	Experimental results	Effect of lattice compression on the change of ^{7}Be decay rate (Qualitative result)
Pd (FCC lattice constant = 3.89Å; Electron affinity = 0.56 eV) *Compared to* **Au** (FCC lattice constant = 4.08Å; Electron affinity = 2.31eV)	0.3%	$(0.8 \pm 0.2)\,\%$	$\sim 0.5\%$
Pt (FCC lattice constant = 3.92Å; Electron affinity = 2.12 eV) *Compared to* **Al** (FCC lattice constant = 4.05Å; Electron affinity = 0.43eV)	−0.4%	$(0.17 \pm 0.13)\,\%$	$\sim 0.5\%$

Recently, the effect of lattice compression on the decay rate of ^{7}Be was observed [15] more directly by implanting ^{7}Be in the small Pd (electron affinity = 0.56 eV) and much larger Pb (electron affinity = 0.35 eV) lattices [14]. Since the electron affinities of Pd and Pb are very small and similar, we find from TB-LMTO calculations [29,30] that the change of the decay rate of ^{7}Be implanted in Pd and Pb due to the effect of different electron affinities would be negligible ($< 0.1\%$). So, the observed increase $[(0.82 \pm 0.16)\%]$ of ^{7}Be decay rate in Pd compared to that in Pb could be attributed to the effect of compression [15]. In order to determine the effect of compression on the electron density at ^{7}Be nucleus, we performed WIEN2k [17,18] density functional calculations for ^{7}Be atoms implanted in the interstitial spaces of the Pd and Pb lattices. To approximately consider the effect of random implantations in a very small percentage of interstitial octahedral and tetrahedral vacancies, we combined two adjacent lattices to form a super lattice and a ^{7}Be atom was placed in either the octahedral or tetrahedral vacancy with a periodic boundary condition. The effect of lattice deformation due to the insertion of ^{7}Be was considered by minimizing the forces on the atoms of the lattice along with minimizing the total energy. We find that WIEN2k predicts only $\sim$0.2% faster decay rate of ^{7}Be in Pd compared to that in Pb due to the compressional effect in the smaller Pd lattice. However, experimentally, a much larger increase $(0.82 \pm 0.16)\%$ [15] of ^{7}Be decay rate in Pd lattice compared to that in Pb lattice was seen and hence, the experimentally observed much faster decay rate under compression could not be understood by the state-of-the-art calculations.

3.3 Implantation of high Z elements in the small and large lattices

As discussed earlier, in the case of implantation of heavier electron capturing nuclei such as ^{109}In and ^{110}Sn in Au and Pb lattices, the observed relatively large increase of electron-capture nuclear decay rate in the small Au lattice is expected to be primarily because of the compressional effect of the lattice. However, the increase of decay rates of ^{109}In and ^{110}Sn due to the lattice compression is expected to be much smaller [10] compared to the corresponding situation for ^{7}Be. The density functional code, WIEN2k calculates on the order of $10^{-3}\%$ change of electron density at ^{109}In and ^{110}Sn nuclei for the implantation of ^{109}In and ^{110}Sn atoms in Au versus Pb lattices. Such a change is much smaller than the accuracy expected from the WIEN2k code.

3.4 Calculations for atom in an impenetrable spherical box

We performed density functional calculations by confining the radioactive atom to an impenetrable spherical box and reducing the dimensions of the impenetrable box to simulate the effect of compression. The assumption of the impenetrable box is expected to give an upper limit for the fractional increase of the electron density at the nucleus $[\Delta\rho(0)/\rho(0)]$. In this method, the atom was confined to an impenetrable spherical box of radius R_c and the fractional increase of the electron density at the nucleus $[\Delta\rho(0)/\rho(0)]$ was calculated by reducing the radius of the box [31,32]. Hence, Kohn and Sham equations were solved subjected to Dirichlet boundary conditions:

$$\rho(\mathbf{r}) = \begin{cases} \rho(\mathbf{r}) & if\ r < R_c \\ 0 & if\ r \geq R_c \end{cases}.$$

Where $\rho(\mathbf{r})$ denotes the electron density at $\mathbf{r}$. Radial Kohn and Sham equations were numerically solved [31] using CONFATOM (confined atoms) code [31]. The value of the electron density at the nucleus was computed by extrapolation. The exchange-correlation func-

tionals used in this code were obtained from the XCFun DFT library [32]. The code used a point nucleus and non-relativistic wave function for the electrons. As the radius of the spherical box (R_C) was reduced, the total electronic kinetic energy $[(E_{kin})_{Total}]$ and the electron density at the nucleus $[\rho(0)]$ increased. An approximate linear relationship between $[\rho(0)]^{2/3}$ and total electronic kinetic energy of the atom $(E_{kin})_{Total}$ has been found for values of R_C smaller than the empirical radius (2.8 Bohr unit) of the indium or tin atom. In order to calculate the fractional increase of the electron density at the nucleus $[\Delta\rho(0)/\rho(0)]$ for the implanted indium or tin atoms in Pb and Au lattices, the increase in total electronic kinetic energy $[\Delta(E_{kin})_{Total}]$ of the implanted indium or tin atom in the smaller Au lattice versus larger Pb lattice was calculated using density functional code TB-LMTO [29,30] that performs all electron calculations and considers the lattice structure of the solids. Then the linear relationship between $[\rho(0)]^{2/3}$ and total electronic kinetic energy of the atom $(E_{kin})_{Total}$ as obtained from CONFATOM code [31] by putting the atom in an impenetrable spherical enclosure ($R_C < 2.8$ Bohr Unit) was used to calculate the fractional increase of the electron density at the nucleus. In the case of implantation of ^{109}In or ^{110}Sn in Au and Pb lattices, the fractional increase of electron density at the nucleus for the implantation in the smaller Au lattice is $\Delta\rho(0)/\rho(0) \approx 0.0004$ or 0.04% and hence the decay rate in the smaller Au lattice is expected to be $\approx$ 0.04% faster compared to that in Pb. The assumption of an impenetrable spherical box is obviously an extreme assumption and the fractional increase of electron density at the nucleus obtained from this model is an upper limit, whereas the WIEN2k code performs much more rigorous calculations. However, this upper limit (0.04%) is also very small and show a negligible increase of decay rate of ^{109}In or ^{110}Sn in different lattice environments. In an overall sense, the results are qualitatively similar to those obtained by Lee and Steinle-Neumann [10] for ^{40}K under high pressure using density functional WIEN2k code [17]. So, we find that in the case of high Z elements such as ^{109}In and ^{110}Sn, the density functional codes underpredict the experimentally measured fractional increase of decay rate ($\Delta\lambda/\lambda$) by at least an order of magnitude.

3.5 Effect of finite nuclear size and quantum electrodynamics (QED)

The effects of finite nuclear size and quantum electrodynamics (QED) are not included in WIEN2k [17,18] or TB-LMTO [29,30] density functional codes. On the other hand, the density functional codes that include the effects of finite nuclear size and QED do not consider a crystal structure and are generally applicable for an isolated atom. We have approximately estimated the effects of finite nuclear size and QED on the fractional increase of electron density at the nucleus $[\Delta\rho(0)/\rho(0)]$ by using a modified density functional code. At first, we obtained the electrostatic lattice potential seen by the relevant atom in the corresponding lattice structure using WIEN2k code [17]. WIEN2k gives this lattice potential in a tabular form at different distances from the atomic nucleus. However, the electrostatic potentials have been obtained assuming point nuclei. The effect of finite nuclear size and QED would affect this potential only very close to a nucleus, whereas, the distant nuclei could be considered as point nuclei and their effect is already included in the lattice potential. The calculation of the finite nuclear size effect has been carried out using a two parameter Fermi model [33] of the nuclear charge distribution as given below:

$$\rho(r) = \frac{N}{1+\exp(\frac{r-c}{a})} \tag{2}$$

where $a = \frac{2.3}{4ln3}$,

$$c = \frac{1}{\sqrt{3}}\left[\left(4\pi^4a^4 - 10\left(r_{rms}^2\right)\pi^2a^2 + \frac{25}{4}(r_{rms}^2)^2\right)^{1/2} - 5\pi^2a^2 + \frac{5}{2}(r_{rms}^2)\right]^{1/2}$$

and $N = \frac{3}{4\pi c^3}\left(1+\frac{\pi^2a^2}{c^2}\right)^{-1}$, where r_{rms} is the root-mean-square nuclear charge radius. $\rho(r)$ has been normalized as follows: $\int_0^\infty drr^2\rho(r) = 1$.

The corresponding Coulomb potential $V_{Coulomb\_finite}(r)$ has been calculated both inside and outside the nucleus. Regarding the QED corrections, the first order correction in α (fine structure constant) comprises two corrections—vacuum polarization and self-energy. From the atomic QED calculations, it is well known [34] that these two corrections for low-lying orbitals have the same order of magnitude with the opposite sign and so, tend to cancel each other. The leading contribution (more than 90%) of the vacuum polarization effect can be described by the local Uehling potential [35]. However, the calculation of self-energy term is rather complicated because of the non-locality of the self-energy operator. In this work, we have only evaluated vacuum polarization correction using Uehling potential. Since we find that the vacuum polarization correction is negligible and much smaller than the uncertainties (~0.1%) of the density functional calculations, we skip the evaluation of the self-energy term that requires much more involved calculations. We have evaluated vacuum polarization contribution using Uehling potential [35] given by

$$U_{VP}^{UE}(r) = -\frac{2\alpha^2Z}{3\pi r}\int_0^\infty dr_1 4\pi r_1\rho(r_1)\int_1^\infty dt\left(1+\frac{1}{2t^2}\right)\frac{\sqrt{t^2-1}}{4t^3}\{exp(-2|r-r_1|t) - exp(-2|r+r_1|t)\}$$

Table 2 Comparison of density functional calculations (including the effect of nuclear size and vacuum polarization) with the experimental results

Change of decay rate of	Experimental Results	Calculations
^{7}Be under external pressure ($P \leq 27$ GPa) on ^{7}BeO crystal	$(2.2 \pm 0.1) \times 10^{-4} P$	$\approx 0.6 \times 10^{-4} P$
^{7}Be in Pd versus Pb lattices	$(0.82 \pm 0.16)\,\%$	$\approx 0.2\%$
^{109}In in Au versus Pb lattices	$(1.00 \pm 0.17)\,\%$	$< 0.1\%$
^{110}Sn in Au versus Pb lattices	$(0.48 \pm 0.25)\,\%$	$< 0.1\%$

where Z and $\rho(r_1)$ denote the nuclear charge and the normalized nuclear charge distribution function given by Eq. (2). The total potential has been taken as $V_{total}\,(r) = V_{\text{Coulomb\_finite}}\,(r) + U_{VP}^{UE}(r)$. The lattice potential very close to an atomic nucleus is dominated by the Coulomb potential of the nucleus and a point nucleus has been assumed in the density functional WIEN2k code. So, the lattice potential very close to the atomic nucleus of the implanted atom (such as ^{7}Be, ^{109}In or ^{110}Sn) in the lattice has been corrected by replacing the potential obtained from WIEN2k code with $V_{\text{total}}\,(r)$ to account for the finite nuclear size and vacuum polarization effects. Then this modified lattice potential (obtained in a tabular form) was used to solve the relativistic Dirac equation for the atomic electrons of an isolated atom using the density functional technique. The electron density at the nucleus has been obtained by averaging over the nuclear volume.

As expected, we find that the finite nuclear size and vacuum polarization have no significant effect on the electron density at the beryllium nucleus, when ^{7}BeO lattice is compressed by an external pressure up to 27 GPa or^{7}Be is implanted in Au, Pd, Al or Pt lattices. The beryllium nucleus is very small and the electronic orbitals of beryllium atom are relatively far away from the nucleus, because of the lower nuclear charge. So, the calculated fractional increase of electron density $[\Delta\rho(0)/\rho(0)]$ at the ^{7}Be nucleus and the corresponding fractional increase of the electron-capture nuclear decay rate $\Delta\lambda/\lambda$ of ^{7}Be under compression remain essentially the same as calculated earlier using density functional WIEN2k code [17,18] with the assumption of the point nuclei.

As the size of the nucleus increases for the higher atomic number (Z) nucleus and the inner electronic orbitals come closer to the nucleus, the effect of the finite size of the nucleus on the increase of the decay rate under compression increases. We find that the fractional increase of the electron density averaged over the nuclear volume of indium implanted in the small Au lattice versus large Pb lattice would increase by about a factor of about 2.6 when the point indium nucleus is replaced by a spherical indium nucleus of radius $r = 1.25\times (109)^{1/3}\text{fm} = 6$ fm. So, considering the effect of finite nuclear size, the electron capture nuclear decay rate of indium in Au lattice could be higher compared to that in Pb by $\approx 2.6 \times 10^{-3}\%$ and the upper limit of the increase could be $\approx (2.6 \times 0.04 = 0.1)\%$ assuming the compression of the atom in an impenetrable spherical box. The effect of vacuum polarization on the fractional increase of electron density $[\Delta\rho(0)/\rho(0)]$ of indium (Z = 49) and tin (Z = 50) nuclei under compression has been found to be smaller than the uncertainty of the density functional calculations. Since the self-energy correction should be of the same order of magnitude with opposite sign, we conclude that the finite nuclear size effect is the dominant effect compared to the QED effect. So, considering both the effects of finite nuclear size and QED, the calculated increase of decay rate of ^{109}In implanted in Au versus Pb lattices would be $\approx 2.6 \times 10^{-3}\%$ and the upper limit of such an increase could be $\approx 0.1\%$. We get similar numbers for the increase of decay rate of ^{110}Sn implanted in Au versus Pb lattice. Hence, the calculated increase of decay rate for ^{109}In in Au and Pb is much smaller compared to the observed increases for these cases. The results of our calculations regarding the change of decay rate of electron-capturing radioactive atoms under compression and the corresponding results have been summarized in Table-2, showing large discrepancies between the experimental results and calculations.

3.6 Quantum anti-Zeno Effect

We have looked into the increase of electron capture nuclear decay rate due to the compression-induced quantum anti-Zeno effect to search for the possible reasons of the discrepancies between the density functional calculations and the experimental results. The quantum mechanical time evolution of an unstable compound state shows non-exponential decay in early time, an approximately exponential decay in the intermediate time and a power law behavior with time at a late time [36–39]. The initial nonexponential decay is very slow in early time (proportional to t^2, where t is the decay time) and then becomes oscillatory before settling down to an exponential decay. The repeated observation of an unstable system during its nonexponential decay could either slow down the decay process (known as Zeno effect) or accelerate the decay process (known as anti-Zeno effect) [40]. Both Zeno and anti-Zeno effects have been observed experimentally for the tunneling of trapped cold sodium atoms [41].

The effect of lattice compression should produce quantum anti-Zeno effect, thus accelerating the decay rate of electron capturing nuclei [40]. However, this effect is generally expected to be very small for the compressions achievable in the laboratory experiments.

In the case of the decay of electron capturing ^{7}Be, the initial nonexponential decay time (τ_{ne}) is generally expected to be $\tau_{ne} \sim \hbar/E_{decay} \approx 10^{-22}$ s, where $E_{decay} \sim 1$ MeV is the energy release in the decay. We may consider that the valence 2s electron of ^{7}Be is monitoring the nuclear charge by rotating around the nucleus. As a result of compression, 2s valence electron is pushed towards the nucleus and it rotates faster. At an external pressure of 27 GPa on ^{7}BeO lattice, the kinetic energy of the valence 2s electron increases by ∼1 eV, implying that the time difference between the successive measurements of the nuclear charge by the orbiting valence electron decreases by $\sim 10^{-16}$ s under compression. Hence, the decay rate of ^{7}Be would increase under an external compression of 27 GPa on ^{7}BeO lattice by $\sim (10^{-22}/10^{-16}) \times 100\% = 10^{-4}$ % due to the quantum anti-Zeno effect [40]. In the cases of electron capture decays of ^{109}In and ^{110}Sn, the decay energies (E_{decay}) are 2.016 MeV and 0.631 MeV respectively. The kinetic energy of the orbital electrons of an atom increases when the atom is compressed by implanting it in the interstitial space of a small lattice. Density functional TB-LMTO code [29,30] predicts that the kinetic energy of the orbital electrons of ^{109}In and ^{110}Sn increases by $\Delta E_{kin} \approx (0.2 - 0.3)$ keV, when the atoms are implanted in the small Au lattice (lattice constant = 4.08Å) compared to their implantations in the larger Pb lattice (lattice constant = 4.95Å). So, the decay rates of ^{109}In and ^{110}Sn would increase by $\sim (\frac{\Delta E_{kin}}{E_{decay}}) = 0.01\%$ and $\sim 0.05\%$ respectively in Au compared to that in Pb because of quantum anti-Zeno effect [40]. However, these numbers are still significantly smaller compared to the observations. In this context, we propose that the change of decay rate of electron-capturing ^{163}Ho implanted in the small palladium lattice (lattice constant = 3.89Å) versus large lead lattice (lattice constant = 4.95Å) could be an interesting case. ^{163}Ho decays to ^{163}Dy by the electron capture process and the decay energy is $E_{decay} = 2.55$ keV only. According to the density functional TB-LMTO code [29,30], the increase of the kinetic energy of the implanted Ho atom in the small palladium lattice compared to the large lead lattice is $\approx 0.2 - 0.3$ keV. Thus, according to the quantum anti-Zeno effect, the electron-capture nuclear decay rate of ^{163}Ho in palladium could be ∼10% faster compared to that in the larger lead lattice. The estimate for a precise increase of the decay rate due to the quantum anti-Zeno effect would be discussed in a future publication.

Another point is that the duration of the initial nonexponential decay time could be substantially longer ($\sim 10^{-19}$–10^{-16} s) in certain models of quantum measurement [36,42,43]. The effect of such a long initial nonexponential decay time on the increase of decay rate under compression has not yet been studied. However, Fonda et al. [36] suggested that the environment performs repeated measurement on the decaying system at random times. As a result of such random interactions with the environment, the decay rate of a nucleus could be modified by a measurable percentage ∼ (1-10)% compared to the theoretical decay rate of the free nucleus, because of the relatively long initial nonexponential decay time.

4 Astrophysical and geophysical implications

We find that the observed relatively large increase of decay rate of electron capturing nuclei under compression cannot be understood by the state-of-the-art density functional or Hartree-Fock calculations. The electron capture by ^{7}Be nuclei is taking place at the center of the Sun at a pressure of 26.5 million GPa and at a temperature of $T = 1.5 \times 10^{7}$ K. Solar neutrino flux from ^{7}Be electron capture reaction in the Sun was recently measured on Earth and found to be in agreement with the standard solar model and neutrino oscillation calculations [44]. However, the solar neutrino flux from ^{7}Be at the solar core is essentially independent of the ^{7}Be electron capture rate at the solar core and depends strongly on the branching between ^{3}He+^{3}He and ^{3}He+^{4}He reaction rates at the solar core [45]. So, the agreement between the measured and calculated ^{7}Be neutrino flux does not imply the accuracy of the calculated ^{7}Be electron capture rate at the solar core. On the other hand, ^{8}B solar neutrino flux is inversely proportional to the ^{7}Be electron capture rate at the solar core. ^{8}B solar neutrino flux (including all neutrino flavors) on Earth was measured accurately by Sudbury Neutrino Observatory (SNO) experiment and found to be $\Phi_{\nu}(^{8}B) = 5.05^{+0.19}_{-0.20} \times 10^{6} cm^{-2} s^{-1}$ [46], in agreement with the calculated ^{8}B solar neutrino flux $\Phi_{\nu\_cal}(^{8}B) = 5.05^{+1.01}_{-0.81} \times 10^{6} cm^{-2} s^{-1}$ from the Standard Solar Models [47]. However, the calculated $\Phi_{\nu\_cal}(^{8}B)$ has large uncertainties (∼20%). This large uncertainty in the calculation of $\Phi_{\nu\_cal}(^{8}B)$ comes from the uncertainties of the heavy element abundances, proton capture rate of ^{7}Be and several other reaction rates in the Sun [45,48]. The electron capture decay rate [R(e)] of ^{7}Be at the solar core has been calculated by employing density matrix technique and is believed to be accurate within 2%. Adelberger et al. [48] considered the measured variations of ^{7}Be decay rate in different chemical environments and concluded that the assigned uncertainty of 2% on the electron capture decay rate [R(e)] of ^{7}Be at the solar core is sufficient to include the variation of the extracted relevant matrix element (obtained from the terrestrial experiments) due to the effect of the electron affinities of different media. Das and Ray [9] also arrived at a similar conclusion from their analysis. However, this conclusion did not consider the measured unexpectedly large increases of ^{7}Be decay rate under compression and the consistent underpredictions of the density functional and Hartree-Fock calculations to account for such effects. Hence, it is conceivable that the standard density matrix and solar model calculations of the electron capture decay rate

of ^{7}Be at the solar core at a pressure of 26.5 million GPa might be underpredicting the actual decay rate and hence, the 2% uncertainty assigned to the calculated ^{7}Be decay rate at the solar core[R(e)] is questionable. Considering the underprediction by the density functional calculations for the compressions achieved at the laboratory experiments, the uncertainty on the calculated electron-capture nuclear decay rate of ^{7}Be at the solar core [R(e)] could be as high as ∼10% [15].

The electron capture process plays a crucial role in the creation of heavy elements during the merger of neutron stars and supernova explosion. The electron-capture nuclear decay rates in these extreme conditions under very high pressure and temperature are calculated by the standard density matrix techniques. The effect of quantum anti-Zeno effect is generally not included in such calculations. However, the compressional energy (∼MeV) under such extreme conditions is expected to be comparable to the nuclear decay energy, thus affecting the electron capture decay nuclear rate due to quantum anti-Zeno effect. Moreover, the effect of initial long nonexponential decay time [36] on the change of decay rate in such extreme environments is not known. Hence, a good theoretical understanding of the increase of electron capture decay rate under compression is required to properly calculate the electron capture nuclear decay rates during the merger of neutron stars and supernova explosions.

The electron-capture nuclear decay of ^{40}K in the outer and inner cores of the Earth at a pressure of ∼ (136-330) GPa plays an important role in the production of a large amount of heat on the order of several Terawatts [49,50]. This large amount of heat is important in determining the thermal and tectonic evolution of the earth. The estimate of the decay rate of ^{40}K at a high pressure at the core of the Earth and the corresponding production of heat would be affected by our observation of the discrepancy between the calculated and measured decay rates at a high pressure.

5 Conclusions

The density functional calculations provide a reasonable explanation of the change of ^{7}Be decay rate in media of different electron affinities [7,9,10]. In this paper, we have focused on understanding the increase of electron capture nuclear decay rate of ^{7}Be due to the application of the external pressure on the ^{7}BeO lattice as well as the increase of decay rate of different electron capturing nuclei due to the compression experienced by the corresponding implanted atoms in a small lattice. We find that the conventional approaches based on the density functional and Hartree-Fock calculations fail to account for the observations. We have included the finite nuclear size and quantum electrodynamics (QED) effects and still fail to explain the observations. Finite nuclear size effect has been found to be much more important than the QED effects for higher Z nuclei. QED effects have been found to be negligible up to Z = 50 and are expected to be smaller than the uncertainties (∼ 0.1%) of the density functional calculations. Quantum anti-Zeno effect is generally believed to produce negligible effect. However, the quantum anti-Zeno effect could produce relatively significant increase (∼10%) of the electron capture decay rate of ^{163}Ho implanted in the small palladium lattice versus large lead lattice, because of the small decay energy (2.55 keV) of ^{163}Ho. Moreover, the effect of relatively longer initial nonexponential decay time for the radioactive decay, as proposed by several models of the quantum measurement, on the electron capture nuclear decay rate under compression is still not known. It is important to understand the observed relatively large increase of decay rate under compression because of its potential implication in the creation of heavy elements and solar neutrino problem as well as for geoscience.

Acknowledgements Two of us, NA and ML want to thank to J. Garza for his useful comments and for allowing us to use his CONFATOM code for confined many electron atoms. A. Ray acknowledges financial assistance from Science and Engineering Research Board, Government of India, Grant Nos. CRG/2020/003237 and EMR/2016/001914.

Author contributions

All the authors have contributed equally in the preparation of the manuscript.

Data Availibility Statement This manuscript has no associated data or the data will not be deposited. [Authors' comment: All the calculated results were generated by the authors and are available upon request. There is no supplementary data sheet with this paper.]

References

1. W. Jaskólski, Phys. Rep **271**, 1 (1996)
2. W. Bambynek, H. Behrens, M.H. Chen, B. Crasemann, M.L. Fitzpatrick, K.W.D. Ledingham, H. Genz, M. Mutterer, R.L. Intemann, Rev. Mod. Phys. **49**, 77 (1977)
3. E. Segre, C.E. Weigand, Phys. Rev. **75**, 39 (1949)
4. J.J. Kraushaar, E.D. Wilson, K.T. Bainbridge, Phys. Rev. **90**, 610 (1953)
5. H.W. Johlige, D.C. Aumann, H.J. Born, Phys. Rev. C **2**, 1616 (1970)
6. G.T. Emery, Ann. Rev. Nucl. Sci. **22**, 165 (1972)
7. A. Ray, P. Das, S.K. Saha, S.K. Das, B. Sethi, A. Mookerjee, C. BasuChaudhuri, G. Pari, Phys. Lett. B **455**, 69 (1999)
8. T. Ohtsuki, H. Yuki, M. Muto, J. Kasagi, K. Ohno, Phys. Rev. Lett. **93**, 112501 (2004)
9. P. Das, A. Ray, Phys. Rev. C **71**, 025801 (2005)
10. K.M.M. Lee, G. Steinle-Neumann, Earth Planet Sci lett **267**, 628 (2008)

11. W.K. Hensley, W.A. Bassett, J.R. Huizenga, Science **181**, 1164 (1973)
12. L.-G. Liu, C.-A. Huh, Earth Planet. Sci. Lett. **180**, 163 (2000)
13. L.I. Cheng-Bo, Z.H.O.U. Shu-Hua, L.I.U. Zhi-Yi, M.E.N.G. Qiu-Ying, Z.H.O.U. Jing, L.I. Xiao-Mei, F.U. Yuan-Yong, W.E.N. Qun-Gang, H.U. Shou-Yang, Chin. Phys. Lett. **27**, 012301 (2010)
14. www.webelement.com
15. A. Ray, A.K. Sikdar, P. Das, S. Pathak, J. Datta, Phys. Rev. C **101**, 035801 (2020)
16. A. Ray, P. Das, S.K. Saha, A. Goswami, A. De, Phys. Lett. B **679**, 106 (2009)
17. P. Blaha, K. Schwarz, G.K.H. Madsen, D. Kvasnicka, J. Lutz, *WIEN2K: An Augmented Plane Wave Local Orbital Program for Calculating Cristalproperties* (TechnischeUniversitat, Wien, Austria, 2001)
18. P. Blaha, K. Schwarz, F. Tran, R. Laskowski, G.K.H. Madsen, L.D. Marks, J. Chem. Phys. **152**, 074101 (2020)
19. R. W. G. Wyckoff, Crystal Structures, Vol-2, Inorganic Compounds RX_n, R_nMX_2, R_nMX_3, Interscience Publishers, a division of John Wiley and Sons, New York, London, Sydney
20. F. Tran, J. Stelzl, P. Blaha, J. Chem. Phys. **144**, 204120 (2016)
21. G.-X. Zhang, A.M. Reilly, A. Tkatchenko, M. Scheffler, New J. Phys. **20**, 063020 (2018)
22. Carl F. Cline, Douglas R. Stephens, J. Appl. Phys. **36**, 2869 (1965)
23. A.V. Bibikov, A.V. Avdeenkov, I.V. Bodrenko, A.V. Nokolaev, E.V. Tkalya, Phys. Rev. C **88**, 034608 (2013)
24. L. Kong, F.A. Bischoff, E.F. Valeev, Chem. Rev. **112**, 75 (2012)
25. A. Szabo, N.S. Ostlund, *Modern Quantum Chemistry* (McGraw-Hill, New York, 1989)
26. Y. Mori, N. Niiya, K. Ukegava, T. Mizuno, K. Takarabe, A.L. Ruoff, Phys. Status Solidi B **241**, 3198 (2004)
27. A.P. Jephcoat, R.J. Hemley, H.K. Mao, R.E. Cohen, M.J. Mehl, Phys. Rev. B **37**, 4727 (1988)
28. A. Ray, P. Das, Phys. Rev. C **90**, 019801 (2014)
29. O.K. Andersen, O. Jepsen, D. Glotzl, *Highlights of Condensed MatterTheory* (North-Holland, New York, 1985)
30. O.K. Andersen, Z. Pawlowska, O. Jepsen, Phys. Rev. B **34**, 5253 (1986)
31. J. Garza, R. Vargas, A. Vela, Phys. Rev. E **58**, 3949 (1998)
32. J. Garza, R. Vargas, N. Aquino, K.D. Sen, J. Chem. Sci. **177**, 379 (2005)
33. V.M. Shabaev, J. Phys. B **26**, 1103 (1993)
34. P.J. Mohr, G. Plunien, G. Soff, Phys. Rep. **293**, 227 (1998)
35. E.A. Uehling, Phys. Rev. **48**, 55 (1935)
36. L. Fonda, G.C. Ghirardi, A. Rimini, Rep. Prog. Phys. **41**, 587 (1978)
37. D. Home, *Conceptual Foundation of Quantum Physics* (Plenum, New York, 1997)
38. L.A. Khalfin, Zh Eksp, Teor. Fiz. **33**, 1371 (1957)
39. L.A. Khalfin, Zh Eksp, Sov. Phys. JETP **6**, 1053 (1958)
40. A.G. Kofman, G. Kurizki, Nature (London) **405**, 546 (2000)
41. M.C. Fischer, B. Gutierrez-Medina, M.G. Raizen, Phys. Rev. Lett. **87**, 040402 (2001)
42. A. Ray, A.K. Sikdar, Phys. Rev. C **94**, 055503 (2016)
43. W.H. Zurek, Rev. Mod. Phys. **75**, 715 (2003)
44. G. Bellini et al., Phys. Rev. Lett. **107**, 141302 (2011)
45. E.G. Adelberger et al., Rev. Mod. Phys. **70**, 1265 (1998)
46. B. Aharmim et al., Phys. Rev. C **81**, 055504 (2010)
47. J.N. Bahcall, M.H. Pinsonneault, S. Basu, Astrophys. J. **555**, 990 (2001)
48. E.G. Adelberger et al., Rev. Mod. Phys. **83**, 195 (2011)
49. K.K.M. Lee, R. Jeanloz, Geophys. Lett. **30**, 2212 (2003)
50. https://en.wikipedia.org/wiki/Earth%27s_internal_heat_budget